Intragrain charge transport in kesterite thin films—Limits arising from carrier localization

Hannes Hempel,[1,a)] Alex Redinger,[1] Ingrid Repins,[2] Camille Moisan,[3] Gerardo Larramona,[3] Gilles Dennler,[3] Martin Handwerg,[4] Saskia F. Fischer,[4] Rainer Eichberger,[5] and Thomas Unold[1,b)]

[1]*Department Structure and Dynamics of Energy Materials, Helmholtz-Zentrum Berlin für Materialien und Energie GmbH, Hahn-Meitner-Platz 1, 14109 Berlin, Germany*
[2]*National Renewable Energy Laboratory, 15013 Denver West Parkway, Golden, Colorado 80401-3305, USA*
[3]*IMRA Europe SAS, 220 rue Albert Caquot BP213, 06904 Sophia Antipolis Cedex, France*
[4]*Novel Materials Group, Humboldt-Universität zu Berlin, 12489 Berlin, Germany*
[5]*Institute for Solar Fuels, Helmholtz-Zentrum Berlin für Materialien und Energie GmbH, Hahn-Meitner-Platz 1, 14109 Berlin, Germany*

(Received 3 August 2016; accepted 8 October 2016; published online 3 November 2016)

Intragrain charge carrier mobilities measured by time-resolved terahertz spectroscopy in state of the art $Cu_2ZnSn(S,Se)_4$ kesterite thin films are found to increase from 32 to 140 $cm^2 V^{-1} s^{-1}$ with increasing Se content. The mobilities are limited by carrier localization on the nanometer-scale, which takes place within the first 2 ps after carrier excitation. The localization strength obtained from the Drude-Smith model is found to be independent of the excited photocarrier density. This is in accordance with bandgap fluctuations as a cause of the localized transport. Charge carrier localization is a general issue in the probed kesterite thin films, which were deposited by coevaporation, colloidal inks, and sputtering followed by annealing with varying Se/S contents and yield 4.9%–10.0% efficiency in the completed device. [http://dx.doi.org/10.1063/1.4965868]

I. INTRODUCTION

Kesterite $Cu_2ZnSn(S,Se)_4$ materials have been intensely investigated as thin solar cell absorber materials during the last years. In spite of the close structural similarity with the chalcopyrite $Cu(In,Ga)Se_2$, significantly lower conversion efficiencies up to about 12.7%[1] have been achieved, compared to more than 22.6% for solar cells based on the latter material. So far, the open-circuit voltage deficit has been identified as the main bottle neck but charge carrier dynamics is not very well understood yet. The mobility of charge carriers is a key property of semiconductor materials, in particular, for their application in various functional devices, such as transistors, photodetectors, and solar cells. In solar cell devices, a large minority carrier mobility ensures long diffusion length and good carrier collection. However, the measurement of the minority carrier mobility is challenging and not accessible with Hall-effect measurements where majority carriers are probed.[2–7] Moreover, the in-plane mobility is measured which is in the case of polycrystalline thin films very different from out of plane mobilities, since grain boundaries are severely influencing the measurements. In order to estimate minority carrier mobilities in kesterite thin films, a combination of internal quantum efficiency (IQE), capacitance-voltage (CV), and time-resolved photoluminescence (TRPL) measurements[8,9] as well as time-resolved terahertz spectroscopy (TRTS)[10] was used before. The IQE-CV-TRPL derived mobilities are in principle also affected by grain boundaries, in particular, by horizontal grain boundaries that lie in the transport path. The method also relies on a number of simplifying assumptions necessary for the analysis of the IQE, CV, and TRPL measurements and requires full device structures.

II. KESTERITE SAMPLES

In this work, we examine the properties of the charge carrier transport in kesterite-type $Cu_2ZnSn(S,Se)_4$ thin films by contactless TRTS, which probes the charge carrier transport on the nm-scale. To be able to generalize, we chose kesterite thin films from different deposition techniques as well as with different Se/S contents. In order to probe relevant thin films with respect to solar cells, only absorber layers that yielded devices with efficiencies between 4.9 and 10% were selected. The composition, the deposition technique, and the solar cell efficiency are summarized in Table I. Further, it contains the intragrain value of the sum of electron and hole mobility μ_{e+h} and localization strength c_1 as they are derived in the subsequent Section III.

The probed absorber was grown on molybdenum-coated glass substrates, which prohibits more commonly used transmission TRTS measurements and complicates reflection TRTS analysis [submitted]. Therefore, all of the absorbers with exception of the sample HZB-Se were lifted off the molybdenum and have a 2 mm thick epoxy film as a new substrate. We chose the lift-off method over a deposition on THz-transparent substrates in order to maintain the deposition conditions and material constraints relevant for kesterite

a)hannes.hempel@helmholtz-berlin.de
b)unold@helmholtz-berlin.de

TABLE I. Sample information.

Sample	Se/(Se + S)	Cu/(Zn + Sn)	Zn/Sn	Deposition method	η (%)	μ_{e+h} (cm^2/V s)	c_1	Reference
NREL	1	0.73	1.6	Coevaporation	7.2	140	−0.65	11
HZB-Se	1	0.7	1.0	Sputtering	7.0	100	−0.71	12
IMRA	0.6	0.83	1.12	Nano colloid ink	10.0	90	−0.72	13 and 14
HZB-S	0	0.80	1.22	Coevaporation	4.9	32	−0.76	15

solar cells. In contrast, the use of a substrate without a molybdenum layer would influence the sodium supply, substrate temperature, and nucleation conditions, which all may affect carrier transport in kesterite thin films.[2,5]

A SEM cross-section of one of the NREL sample is shown in Fig. 1. Rather large dark grains ranging from 1–2 μm and rather small bright grains at the Mo substrate as well as a bright capping layer are observed. The dark grain can be attributed to $Cu_2ZnSnSe_4$ and the bright areas to ZnSe. This secondary phase also contributes to the relatively high Zn/Sn ration of 1.6 the sample (Table I) in accordance with recent findings.[16] In Fig. 1, we have also indicated the probing direction and range of different methods that have been employed for the analysis of charge carrier mobilities. While TRTS probes the mobility within single grains, as discussed further below, Hall-effect measurements probe the lateral transport of majority carriers and can be dominated by grain boundary potentials. On the other hand, mobilities derived from combined IQE-CV-TRPL measurements[8,9] probe the vertical transport of minority carriers and thus are also expected to yield mobilities, which are representative for the carrier transport in thin film solar cells.

III. THz-MOBILITY OF NANO-SCALE LOCALIZED CHARGE CARRIERS

TRTS has been described extensively in several reviews.[17–19] We use TRTS in the reflection mode to avoid THz absorption in the substrate off samples.[20–22] It is described in Ref. 23 and based on an amplified Ti-Sapphire laser system which delivers three pulsed laser beams with 805 nm center wavelength, 50 fs pulse with, and 150 kHz repetition rate. In principle, the first 805 nm optical pump pulse generates charge carriers on the former Mo-bonded side of the kesterite thin film with an absorption depth of 500 nm–230 nm for increasing Se content.[24] These additional carriers increase the conductivity of the thin film, which also changes its refractive index.[25] This changed refractive index causes a change in the reflection of the THz probe pulse which is generated by optical rectification of the second 805 nm pulse in a ZnTe crystal. The THz probe pulse is detected by electro optical sampling in a ZnTe crystal by the third 805 nm pulse. Employing a numerical analysis based on the transfer matrix method, we can deduce the mobility of the pump-induced charge carriers from the measured change in THz reflection. The extracted mobility is the complex AC-mobility at THz frequencies that describes the amplitude and phase of the pump-excited charge carrier current driven by the THz probe pulse. The error in the extracted mobility can be estimated to be approximately 20% and consists mainly of uncertainties in the excited carrier concentrations, the layer thicknesses, and the refractive indices as input for the transfer matrix analysis as well as errors from the DC-mobility fit.

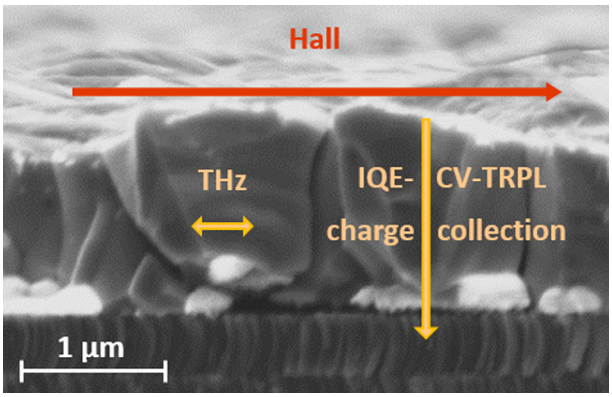

FIG. 1. SEM picture of the NREL kesterite absorber on molybdenum with illustration of the different spatial sensitivities of TRTS, Hall, and IQE-CV-TRPL as charge carrier mobility measurements.

Although the THz probe spot size is ~1 mm on the kesterite films and averages the mobility over that area, the interaction between the THz field and single charge carriers occurs on the nm-scale.[26] We assume the interaction between the single-oscillation THz pulse and the individual charge carriers to take place within one oscillation of $f = 1$ THz. Within that time, the THz field of ~1000 V/cm induces a carrier oscillation of $l_F = \mu E/\omega = 1.6$ nm (Ref. 27) while the charge carrier diffuse a distance $l_D = (\mu k_B T/ef)^{0.5} = 50$ nm, assuming a mobility μ of 1000 cm^2/V s. Together this leads to an interaction length <50 nm for mobilities $\mu < 1000$ cm^2/V s which is far below the grain size of ~1 μm in the probed kesterite thin films (Fig. 1). Therefore, the THz mobilities are intragrain values.

The measured AC-mobilities of the kesterite absorbers are shown in Fig. 2. Despite differences in the absolute values of the real and imaginary parts, all spectra show the same overall trend, with a real part increasing for larger frequencies, and a negative imaginary part. This common shape of the mobility spectra allows us to draw conclusions on the nature of charge transport. Free charge carriers exhibit a Drude-like mobility spectrum, which depends only on the momentum relaxation time τ and the effective charge carrier mass m_{eff}, i.e., $\mu = e\tau/m_{eff}(1 + i\omega\tau)^{-1}$. However, a negative imaginary mobility as measured for the kesterite thin films in Fig. 2 cannot be explained by the Drude model. The negative imaginary mobility is indicative for charge carrier localization, which has been concluded from ps-decay components in transient reflection measurements on sulfur based kesterite single crystals before.[28] To be independent of the physical

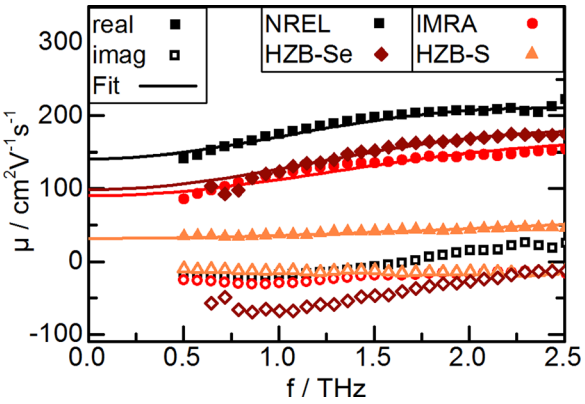

FIG. 2. Imaginary and real AC-mobilities of lift off kesterite absorbers on epoxy (HZB-Se as grown on Mo) measured by reflection TRTS at 20 ps after excitation by 1.6×10^{13} photon flux of per pump pulse. Solid lines are fits with the Drude-Smith model to extrapolate DC mobilities.

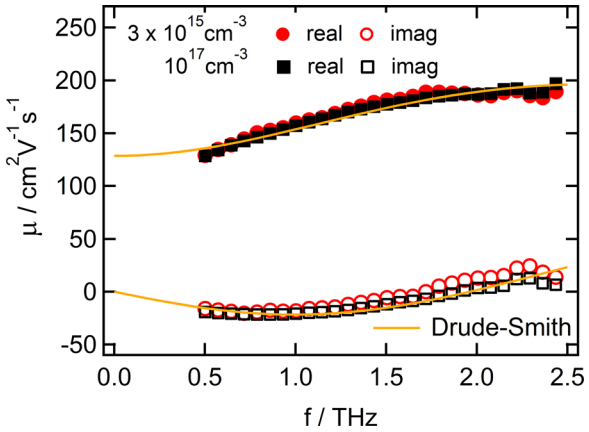

FIG. 3. AC-mobility mobility spectra of the NREL kesterite sample for different photoinduced electron concentrations at the sample surface and with Drude-Smith fit yielding $c_1 = -0.67$, $\tau^* = 46$ fs, and $m_{eff}^* = 0.22$.

model of carrier localization, but to be able to parameterize the mobility and extrapolate the DC-value, the data can be analyzed using the phenomenological Drude-Smith model[29]

$$\mu_{DS} = \frac{e\tau}{m_{eff}(1 + i\omega\tau)}\left(1 + \frac{c_1}{1 + i\omega\tau}\right). \quad (1)$$

Here, the first term describes the free carrier Drude mobility, while the second term and in particular, the localization parameter c_1 describes a continuous transition of the free carrier Drude-like ($c_1 = 0$) mobility from to a highly localized spectrum ($c_1 = -1$). The Drude-Smith model was derived by assuming preferential backscattering of a fraction c_1 of the carriers at their first scattering event, while all subsequent scattering events were assumed to randomize the carrier velocity. As there is no physical reason why charge carriers should scatter backwards at the first scattering event and not at later scattering events, the Drude-Smith model is limited to a phenomenological description of the carrier localization. Despite its lack of microscopic insight, the c_1 parameter has been found to be a good measure for the degree of localization of charge carrier mobility and to enable extrapolation of THz mobilities to DC values.[29] However, in our opinion the momentum relaxation time τ and effective mass m_{eff}^* lose their original physical meanings due to the phenomenological nature of the Drude-Smith model, although we are aware that this is discussed controversially in the TRTS community. If the AC-mobilities are extrapolated to low frequencies using the Drude-Smith model, DC mobility values of 140, 100, 90, and 32 $cm^2/V\,s$ are obtained for the samples NREL, HZB-Se, IMRA, and HZB-S, respectively. These values compare well with the 70 $cm^2/V\,s$ which has been obtained previously for a mixed Se/S kesterite thin film by TRTS.[10]

The mobility modeled with Equation (1) is shown in Fig. 3 for the NREL sample. It can be seen that a very good fit of the THz mobility is obtained for $c_1 = -0.67$, $m_{eff}^* = 0.22$, and $\tau = 46$ fs, where the c_1 value indicates a strong localization. This localization takes place on a length scale below 50 nm and is therefore not caused by dimension of the grains ($\sim 1\,\mu m$). The m_{eff*} parameter of 0.22 is far from the predicted value of the effective electron mass of 0.08 in kesterite[30] and illustrates that m_{eff*} does not represent the real effective charge carrier mass in the Drude-Smith model. The parameter τ is in the expected range of a typical momentum relaxation time but also should not be directly associated with the microscopic scattering time.

IV. CARRIER LOCALIZATION BY BANDGAP FLUCTUATIONS

Charge carrier localization in kesterite semiconductors may be caused by various phenomena reported previously, among them are grain boundary scattering, bandgap fluctuations,[31] electrostatic potential fluctuations,[32,33] surface band bending,[34] Cu-Zn disorder,[35–37] defect bands,[38,39] and secondary phases.[40] Because of the nm-probing range of the TRTS method, we can exclude grain boundary scattering as the source of localization. Further, it has been shown previously[41] that AC-conductivities as a function of frequency have similar dependencies in disordered solids independent of the details of the disorder which complicates an assignment of the observed localization to one of the former causes. Therefore, we investigate the dependency of carrier localization on pump-induced carrier concentration Δn in order to narrow down the possible explanations. The photoinduced carrier concentration corresponds to the density of excited electrons at the surface of the semiconductor and decreases with the Lambert-Beer law into the sample. Further excited hole and electron concentration are equal right after excitation. In Fig. 3, THz mobility spectra for two strongly differing excited charge carrier concentrations (3×10^{15} and 10^{17} cm^{-3}) are shown, which are indistinguishable within the measurement accuracy. In contrast, mobility spectra of charge carriers localized in potential fluctuations or surface band bending should show a transition to a lower degree of localization due to screening of the potential variations. If we assume that the amplitude of electrostatic potential fluctuations γ_0 in a p-type semiconductor at room temperature is limited by a Debye screening from free charge carriers, the amplitude is proportional to $\gamma_0 \sim (n + \Delta n)^{-1/4}$,[42] where n is the doping density of $\sim 10^{16}$ cm^{-3} estimated by

capacitance–voltage measurements and Δn the induced carrier concentration. For the high excitation density of $10^{17}\,cm^{-3}$, the potential amplitude would be reduced to roughly half of its initial amplitude, which should be observable as a reduced localization of the charge carrier. In a similar manner, also surface band bending is screened by additional free carriers. This indicates that electrostatic potential fluctuations and surface band bending can be excluded as a cause for the measured localization. Secondary phase inclusions with individual charge carrier mobilities can also cause localization in the mobility spectra. The screening of the incident THz field by the mobile charge carriers is inhomogeneous in such a material and using an effective medium approach it has been shown that the observed localization-like THz mobility spectrum should be strongly carrier concentration dependent,[26] which is not observed in kesterite samples.

Due to the employment of pump/probe pulses with a high time resolution of ~100 fs, the conductivity transient can be scanned by TRTS. The photoconductivity transient of the NREL sample in Fig. 4(a) is double exponential with decay times of 100 ps and 2.1 ns. The long decay component is very similar to life time values in kesterite thin films reported for time-resolved photoluminescence. Additionally, the TRTS-derived mobility can be recorded at different pump-probe delays, which enables the detection of carrier mobilities at different times after carrier excitation. Such measurements performed for the NREL sample ($\Delta n = 10^{17}\,cm^{-3}$) show mobility spectra exhibiting carrier localization already 5 ps after the excitation pulse. At further pump-probe delays, the spectra show almost no change and the fitted localization strength c_1 as well as the DC-mobility stay approximately constant as plotted in Fig. 4(b). This shows that carrier localization occurs on a very fast time-scale below 2 ps rather than via long time trapping processes, as would be expected from multiple trapping or multiple hopping.[43] Further, the decay of the photoconductivity in Fig. 4(a) can be assigned to the recombination of the photo excited carriers as the mobility in Fig. 4(b) is constant for times >5 ps.

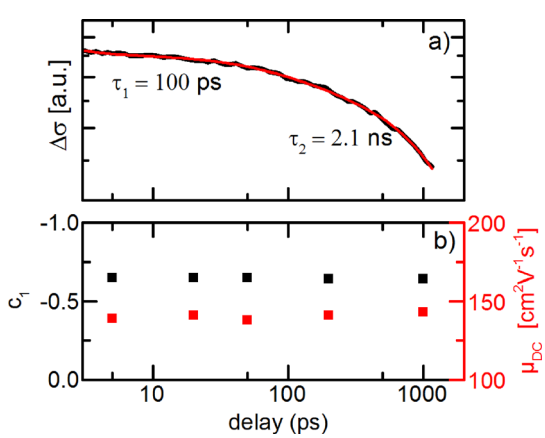

FIG. 4. (a) Transient of the photoinduced conductivity $\Delta\sigma$ and (b) localization strength c_1 and extrapolated DC-mobility μ_{DC} of NREL sample at different delay times after carrier excitation.

Considering the non-stoichiometric composition of the investigated material and the various experimental and theoretical evidence for the presence of bandgap fluctuations caused in particular, by the presence of Cu-Zn disorder, we believe that band gap fluctuations are the most likely cause of the carrier localization observed in our measurements. Because of the short interaction length estimated above, these band gap fluctuations must occur on the nm-scale, i.e., below 50 nm. This is in line with compositional fluctuations on the 20 nm scale measured by energy dispersive X-ray spectroscopy in kesterite single crystals.[44]

V. DC-MOBILITIES

The observed localization complicates the assignment of the measured TRTS mobilities to electrons or holes. TRTS is sensitive to all excited charge carriers and therefore measures the sum of electron and hole mobilities, i.e., $\Delta\sigma = e(\mu_n\Delta n + \mu_p\Delta p)$, where $\Delta\sigma$, Δn, Δp, μ_n, and μ_p are the induced conductivity, the induced electron and hole concentrations and the electron and hole mobilities, respectively. In the free carrier description, the THz mobilities would be dominated by the carriers with lower effective mass, which are the electrons in kesterite.[10,30] As the charge carriers in kesterite are not free but localized, it is not *a priori* clear if either electrons or holes are affected more by localization and which species has the higher mobility.

In Fig. 5, we show the TRTS derived mobilities as a function of band gap/selenium content. It can be seen that the mobilities show a monotonic increase with increasing Se content, with highest values slightly above $100\,cm^2/V\,s$. The figure also includes a literature value of a TRTS-derived mobility,[10] which is in excellent agreement with the present study. The values are also similar to mobilities obtained by this method for Cu-poor state-of-art $CuInSe_2$.[45] In addition, the figure includes mobilities obtained from Hall and combined IQE-CV-TRPL measurements reported in the literature.[8,9]

Inspection of Fig. 5 shows that the charge carrier mobilities obtained for kesterite thin films by different methods vary by almost two orders of magnitude, while the variation

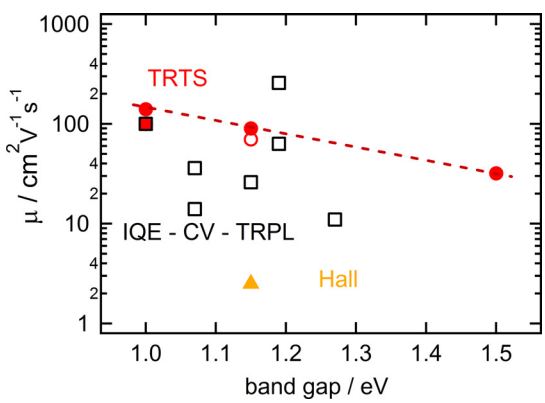

FIG. 5. Extrapolated DC-mobilites from TRTS of kesterite for different bandgaps which are representive for different Se/S contents. Comparison of the mobility measurement by Hall in the IMRA sample and literature values (open symbols) from TRTS[10] as well as an combination of IQE, CV, and TRPL measurements.[8,9] The dashed line indicates higher mobilities for Se rich kesterites.

is significantly smaller (factor 4) if only TRTS-derived values are considered. The mobility derived from the Hall-measurement performed in this study ($\mu = 2.5\,cm^2/V\,s$) is significantly lower than the values obtained from either TRTS or IQE-CV-TRPL, while the values from the latter two methods are of the same order of magnitude. The low mobility obtained from the Hall measurement can be explained either by the fact that the majority carriers (holes) exhibit a significantly lower mobility than electrons in kesterite than electrons or by a dominant influence of grain boundary scattering.

The mobilities derived from IQE-CV-TRPL are higher than the Hall mobility but generally lower than the TRTS-derived values with exception of one data point and show a large variation of values for a given bandgap value (or selenium content). The large variations are likely a consequence of the combined individual errors of the three methods IQE, CV, and TRPL. Especially, the lifetime estimation from the commonly observed non-exponential TRPL decay and the frequency dependent space-charge region width from CV are origins of uncertainties. Further, grain boundaries in the transport direction may reduce the IQE-CV-TRPL derived mobility and as different samples possibly contain different microstructures this may also contribute to the mobility variation. Under this assumption, the highest minority carrier mobilities derived by IQE-CV-TRPL would likely originate from samples where no grain boundaries are present in the transport direction and therefore represent intragrain values.

The intragrain TRTS-mobilities lie right in the middle of the highest minority carrier IQE-CV-TRPL mobilities ($E_g = 1.15\,eV$). This is a strong indication that the TRTS-mobilities are indeed minority carrier (electron) mobilities relevant for the estimation of charge carrier diffusion lengths and that the high value IQE-CV-TRPL derived mobilities are not hindered by grain boundaries. The fact that the TRTS mobilities for higher Se/S contents result in higher mobilities, while still showing localized charge dynamics, leads us to hypothesize that bandgap fluctuations caused by cation disorder are less severe for the material with higher selenium content. The variation in TRTS-mobilities for similar band gap values (or selenium content) is within 20% and shows the high reliability of the method.

VI. CONCLUSION: CONSEQUENCES FOR KESTERITE SOLAR CELLS

From the estimated minority carrier mobilities and typical minority carrier lifetimes found for kesterite samples, the diffusion length for electrons can be estimated using $L = (\mu k_B T \tau/e)^{0.5}$. For a lifetime of $\tau \sim 2.1$ ns measured for the NREL sample by TRTS and the mobility $\mu = 140\,cm^2/V\,s$ we get $L \sim 860$ nm, which is slightly smaller than the film thickness of $d \sim 1\,\mu m$. Therefore, a minor fraction of the photo carriers is not collected in the finished solar cell. An increase in diffusion length to values $L \gg d$ could be achieved by either increasing the minority carrier lifetime and/or by increasing the carrier mobility. If we compare both values to the properties found for CIGSe, then it is apparent that the lifetime in Kesterite is much lower (1–5 ns compared to 50–250 ns) while the mobilities are comparable ($30–140\,cm^2/V\,s$ vs. $100–200\,cm^2/V\,s$). This indicates that the minority carrier mobility is not a real fundamental limit to photocurrent collection and thus device efficiency. On the other hand, an increase of the mobility would still increase the diffusion length and thus increase the efficiency, especially if thicker devices are used in order to maximize absorption also for the longer wavelengths. This could be achieved by reducing the band gap fluctuations, thus reducing localization that has been found in this study to limit the mobilities. Previous studies on stoichiometric $CuInSe_2$ have shown Drude-like charge carrier dynamics with no sign of carrier localization, yielding TRTS-mobilities of up to $1000\,cm^2/V\,s$ (Ref. 46) which in turn compares to mobilities found for epitaxial layers of InP or GaAs where also no charge carrier localization was detected.[47,48]

ACKNOWLEDGMENTS

The authors gratefully acknowledge the Helmholtz Association Initiative and Network Fund (HNSEI-Project) and the Fonds national de la recherche, Project No. 7842175 for the financial support of this work.

[1]J. Kim, H. Hiroi, T. K. Todorov, O. Gunawan, M. Kuwahara, T. Gokmen, D. Nair, M. Hopstaken, B. Shin, Y. S. Lee *et al.*, Adv. Mater. **26**, 7427–7431 (2014).
[2]A. Nagaoka, H. Miyake, T. Taniyama, K. Kakimoto, Y. Nose, M. A. Scarpulla, and K. Yoshino, Appl. Phys. Lett. **104**, 152101 (2014).
[3]E. M. Mkawi, K. Ibrahim, M. K. M. Ali, K. M. A. Saron, M. A. Farrukh, and N. K. Allam, J. Mater. Sci.: Mater. Electron. **26**, 222–228 (2015).
[4]A. Nagaoka, K. Yoshino, H. Taniguchi, T. Taniyama, and H. Miyake, J. Cryst. Growth **354**, 147–151 (2012).
[5]A. R. Wibowo, E. Soo Lee, B. Munir, and K. Ho Kim, Phys. Status Solidi A **204**, 3373–3379 (2007).
[6]D.-H. Kuo and M. Tsega, J. Solid State Chem. **206**, 134–138 (2013).
[7]D.-H. Kuo and W. Wubet, J. Alloys Compd. **614**, 75–79 (2014).
[8]T. Gokmen, O. Gunawan, and D. B. Mitzi, J. Appl. Phys. **114**, 114511 (2013).
[9]C. J. Hages, N. J. Carter, and R. Agrawal, J. Appl. Phys. **119**, 014505 (2016).
[10]G. W. Guglietta, K. R. Choudhury, J. V. Caspar, and J. B. Baxter, Appl. Phys. Lett. **104**, 253901 (2014).
[11]I. Repins, J. Li, A. Kanevce, C. Perkins, K. Steirer, J. Pankow, G. Teeter, D. Kuciauskas, C. Beall, C. Dehart *et al.*, Thin Solid Films **582**, 184–187 (2015).
[12]S. Levcenko, J. Just, A. Redinger, G. Larramona, S. Bourdais, G. Dennler, A. Jacob, and T. Unold, Phys. Rev. Appl. **5**, 024004 (2016).
[13]G. Larramona, S. Bourdais, A. Jacob, C. Chone, T. Muto, Y. Cuccaro, B. Delatouche, C. Moisan, D. Pere, and G. Dennler, J. Phys. Chem. Lett. **5**, 3763–3767 (2014).
[14]G. Larramona, S. Levcenko, S. Bourdais, A. Jacob, C. Chone, B. Delatouche, C. Moisan, J. Just, T. Unold, and G. Dennler, Adv. Energy Mater. **5**, 1501404 (2015).
[15]B.-A. Schubert, B. Marsen, S. Cinque, T. Unold, R. Klenk, S. Schorr, and H.-W. Schock, Prog. Photovoltaics: Res. Appl. **19**, 93–96 (2011).
[16]J. Just, C. M. Sutter-Fella, D. Lätzenkirchen-Hecht, R. Frahm, S. Schorr, and T. Unold, Phys. Chem. Chem. Phys. **18**, 15988–15994 (2016).
[17]P. Jepsen, D. Cooke, and M. Koch, Laser Photonics Rev. **5**, 124–166 (2011).
[18]C. A. Schmuttenmaer, Chem. Rev. **104**, 1759–1780 (2004).
[19]R. Ulbricht, E. Hendry, J. Shan, T. F. Heinz, and M. Bonn, Rev. Mod. Phys. **83**, 543–586 (2011).
[20]D. G. Cooke, F. C. Krebs, and P. U. Jepsen, Phys. Rev. Lett. **108**, 056603 (2012).
[21]D. A. Valverde-Chavez, C. S. Ponseca, C. C. Stoumpos, A. Yartsev, M. G. Kanatzidis, V. Sundström, and D. G. Cooke, Energy Environ. Sci. **8**, 3700–3707 (2015).

[22]F. D'Angelo, H. Nemec, S. H. Parekh, P. Kuzel, M. Bonn, and D. Turchinovich, Opt. Express **24**, 10157 (2016).
[23]H. Hempel, T. Unold, and R. Eichberger, Rev. Sci. Instrum. (submitted).
[24]S. G. Choi, H. Y. Zhao, C. Persson, C. L. Perkins, A. L. Donohue, B. To, A. G. Norman, J. Li, and I. L. Repins, J. Appl. Phys. **111**, 033506 (2012).
[25]P. Kuzel, F. Kadlec, and H. Nemec, J. Chem. Phys. **127**, 024506 (2007).
[26]H. Nemec, P. Kuzel, and V. Sundström, J. Photochem. Photobiol., A **215**, 123–139 (2010).
[27]J. Lloyd-Hughes and T.-I. Jeon, J. Infrared, Millimeter, Terahertz Waves **33**, 871–925 (2012).
[28]L. Quang Phuong, M. Okano, Y. Yamada, A. Nagaoka, K. Yoshino, and Y. Kanemitsu, Appl. Phys. Lett. **103**, 191902 (2013).
[29]N. Smith, Phys. Rev. B **64**, 155106 (2001).
[30]C. Persson, J. Appl. Phys. **107**, 053710 (2010).
[31]J. J. S. Scragg, J. K. Larsen, M. Kumar, C. Persson, J. Sendler, S. Siebentritt, and C. Platzer Björkman, Phys. Status Solidi B **253**, 247–254 (2016).
[32]D. P. Halliday, R. Claridge, M. C. J. Goodman, B. G. Mendis, K. Durose, and J. D. Major, J. Appl. Phys. **113**, 223503 (2013).
[33]T. Gokmen, O. Gunawan, T. K. Todorov, and D. B. Mitzi, Appl. Phys. Lett. **103**, 103506 (2013).
[34]Z. Zhao, G. Niehues, S. Funkner, E. Estacio, Q. Han, K. Yamamoto, J. Zhang, W. Shi, Q. Guo, and M. Tani, Appl. Phys. Lett. **105**, 231104 (2014).
[35]B. G. Mendis, M. D. Shannon, M. C. Goodman, J. D. Major, R. Claridge, D. P. Halliday, and K. Durose, Prog. Photovoltaics: Res. Appl. **22**, 24–34 (2014).
[36]S. Schorr, Sol. Energy Mater. Sol. Cells **95**, 1482–1488 (2011).
[37]J. J. S. Scragg, L. Choubrac, A. Lafond, T. Ericson, and C. Platzer-Björkman, Appl. Phys. Lett. **104**, 041911 (2014).
[38]M. Guc, R. Caballero, K. Lisunov, N. Lpez, E. Arushanov, J. Merino, and M. Leon, J. Alloys Compd. **596**, 140–144 (2014).
[39]A. Nagaoka, H. Miyake, T. Taniyama, K. Kakimoto, and K. Yoshino, Appl. Phys. Lett. **103**, 112107 (2013).
[40]J. Just, D. Lützenkirchen-Hecht, R. Frahm, S. Schorr, and T. Unold, Appl. Phys. Lett. **99**, 262105 (2011).
[41]J. C. Dyre and T. B. Schröder, Rev. Mod. Phys. **72**, 873–892 (2000).
[42]R. A. Street, *Hydrogenated Amorphous Silicon* (Cambridge University Press, 2005), p. 286.
[43]B. Hartenstein, H. Bässler, A. Jakobs, and K. W. Kehr, Phys. Rev. B **54**, 8574–8579 (1996).
[44]J. A. Aguiar, M. E. Erkan, D. S. Pruzan, A. Nagaoka, K. Yoshino, H. Moutinho, M. Al-Jassim, and M. A. Scarpulla, Phys. Status Solidi A **213**, 2392–2399 (2016).
[45]T. Unold, H. Hempel, C. Strothkamper, C. Kaufmann, R. Eichberger, and A. Bartelt, in IEEE 40th Photovoltaic Specialist Conference (PVSC) (2014).
[46]C. Strothkämper, A. Bartelt, R. Eichberger, C. Kaufmann, and T. Unold, Phys. Rev. B **89**, 115204-1 (2014).
[47]H. Nemec, L. Fekete, F. Kadlec, P. Kuzel, M. Martin, J. Mangeney, J. C. Delagnes, and P. Mounaix, Phys. Rev. B **78**, 235206 (2008).
[48]M. C. Beard, G. M. Turner, and C. A. Schmuttenmaer, Phys. Rev. B **62**, 15764–15777 (2000).